Electronic Supplementary Material (ESI) for ChemComm.

Stepwise assembly of an adamantanoid Ru_4Ag_6 cage by control of metal coordination geometry at specific sites.

Alexander J. Metherell and Michael D. Ward

Supporting Information

Preparations of complexes

Preparation of *fac*–[Ru(L^{ph})$_3$][PF_6]$_2$. A mixture of *fac*-[Ru(PyPzH)$_3$](PF_6)$_2$ (0.05 g, 0.05 mmol; preparation in ref. 12a) and intermediate **A** (0.11 g, 0.33 mmol; preparation in ref. S1), Cs_2CO_3 (0.15 g, 0.46 mmol), Bu_4NI (0.10 g, 0.27 mmol) and CH_2Cl_2 (20 cm^3) was heated to reflux in the dark with stirring for 48 h. After cooling to room temperature, excess Cs_2CO_3 was filtered off and the solvent removed by rotary evaporation, before purification of the yellow solid by column chromatography on silica by elution with MeCN–water–saturated aqueous KNO_3 (100:10:5 ratio by volume). After removing acetonitrile by rotary evaporation, excess saturated aqueous KPF_6 was added and the product was extracted from the suspension into dichloromethane. The organic layer was separated, dried over $MgSO_4$, and the solvent removed *in vacuo* to yield *fac*–[Ru(L^{ph})$_3$][PF_6]$_2$ as a yellow solid in 68% yield. Slow diffusion of di-isopropyl ether vapour into a solution of the complex in acetone afforded the product as yellow needles.

^{1}H NMR (400 MHz, CD_3CN): δ 8.58 (1H, ddd, *J* = 4.7, 1.8, 0.8; pendant pyridyl H^6), 8.00 (1H, td, *J* = 8.0, 1.0; pendant pyridyl H^3), 7.83 (1H, d, *J* = 2.2; pendant pyrazolyl), 7.79 (1H, td, *J* = 7.8, 1.8; pendant pyridyl H^4), 7.71 (1H, d, *J* = 2.9; coordinated pyrazolyl), 7.61 (1H, td, *J* = 7.8, 1.4; coordinated pyridyl H^4), 7.27 (1H, ddd, *J* = 7.4, 4.9, 1.1; pendant pyridyl H^5), 7.24 (1H, d, *J* = 8.0; coordinated pyridyl H^3), 7.03 (1H, ddd, *J* = 7.9, 5.7, 1.4; coordinated pyridyl H^5), 6.98 (1H, d, *J* = 2.2; pendant pyrazolyl), 6.94 (1H, d, *J* = 5.7; coordinated pyridyl H^6), 6.88 (2H, d, *J* = 8.2; phenyl H^3), 6.54 (1H, d, *J* = 2.9; coordinated pyrazolyl), 5.91 (2H, d, *J* = 8.2; phenyl H^2), 5.48 (1H, d, *J* = 17.3; CH_2 closer to Ru, 5.29 (2H, s; CH_2 further from Ru), 4.78 (1H, d, *J* = 17.3; CH_2 closer to Ru). ESMS: *m/z* 1424 (M – PF_6)$^+$, 639 (M – 2PF_6)$^{2+}$. Found: C, 54.9; H, 3.9; N, 16.0. $C_{72}H_{60}F_{12}N_{18}P_2Ru$ requires C, 55.1; H, 3.9; N, 16.1%. UV/Vis in MeCN [λ_{max}/nm (10^{-3} ε/M^{-1} cm^{-1})]: 399 (12.6), 282 (64.4), 250 (66.3).

Preparation of [Ru_4Ag_6(L^{Ph})$_{12}$](PF_6)$_{14}$. To a solution of *fac*-[Ru(L^{Ph})$_3$](PF_6)$_2$ (0.023 g, 0.015 mmol) in CH_3CN (1 cm^3) was added a solution of $AgPF_6$ (0.007 g, 0.028 mmol, 1.8 eq) in CH_3CN (1 cm^3). The solution was mixed vigorously for 16h and then evaporated to dryness. The yellow residue was washed with MeOH and dried *in vacuo*. Slow diffusion of di-isopropyl ether vapour into a solution of the complex in acetonitrile afforded the product as yellow blocks. ESMS: *m/z* 2452 {(Ru_4Ag_6(L^{Ph})$_{12}$)(PF_6)$_{11}$}$^{3+}$; 1803 {(Ru_4Ag_6(L^{Ph})$_{12}$)(PF_6)$_{10}$}$^{4+}$; 1678 {(RuAg(L^{Ph})$_3$)(PF_6)}$^+$; 1154 {(Ru_4Ag_6(L^{Ph})$_{12}$)(PF_6)$_8$}$^{6+}$; 892 {($RuAg_2$(L^{Ph})$_3$)(PF_6)$_2$}$^{2+}$; 546 {($RuAg_2$(L^{Ph})$_3$)(PF_6)}$^{3+}$. The vacuum-dried material gave elemental analyses consistent with absorption of large numbers of H_2O molecules. Anal. Calcd for [Ru_4Ag_6(L^{pPh})$_{12}$](PF_6)$_{14}$•9H_2O: C, 43.5; H, 3.3; N, 12.7%. Found: C, 43.8; H, 3.6; N, 12.8%. Yield based on this formulation: ca. 80%.

S1 S. P. Argent, H. Adams, L. P. Harding, T. Riis-Johannessen, J. C. Jeffery and M. D. Ward, *New J. Chem.,* 2005, **29**, 904.

S2 (a) http://spdbv.vital-it.ch; (b) N. Guex and M. C. Peitsch, *Electrophoresis,* 1997, **18**, 2714

Crystallographic data

Crystal data for *fac*-$[Ru(L^{ph})_3][PF_6]_2$•acetone: $C_{75}H_{66}F_{12}N_{18}OP_2Ru$, M = 1626.47 g mol^{-1}, orthorhombic, space group *P*bca, a = 23.2400(17), b = 13.2721(9), c = 47.443(3) Å, U = 14633.5(17) $Å^3$, Z = 8, T = 100(2) K, λ(Mo-Kα) = 0.71073 Å. 38114 reflections were collected ($2\theta_{max}$ = 44°) which after merging afforded 8193 independent reflections with R_{int} = 0.099. Final $R1$ [$I > 2\sigma(I)$] = 0.133; $wR2$ (all data) = 0.310.

Crystal data for $[\{Ru(L^{ph})_3\}_4Ag_6](PF_6)_{14}$: $C_{288}H_{240}Ag_6F_{84}N_{72}P_{14}Ru_4$, M = 7790.59 g mol^{-1}, monoclinic, space group *P*2/n, a = 24.688(3), b = 30.324(4), c = 25.247(3) Å, b = 102.819°, U = 18430(4) $Å^3$, Z = 2, T = 100(2) K, λ(Mo-Kα) = 0.71075 Å. 167655 reflections were collected ($2\theta_{max}$ = 45°) which after merging afforded 24082 independent reflections with R_{int} = 0.065. Final $R1$ [$I > 2\sigma(I)$] = 0.141; $wR2$ (all data) = 0.429.

In both cases crystals scattered weakly due to the complexity of the molecules and the presence of solvation and disorder of solvents / anions; however the quality of the refinement is in each case sufficient to establish the structures and connectivities. Both structures contain a solvent-accessible void containing diffuse electron density that could not modelled satisfactorily and was removed from the final refinement using the SQUEEZE function in PLATON: full details are in the CIFs. The datasets were collected at the EPSRC National Crystallography Service at the University of Southampton (ref. S3) and solved / refined using the SHELX software package (ref. S4).

S3 S. J. Coles and P. A. Gale, *Chem. Sci.,* 2012, **3**, 683.

S4 G. M. Sheldrick, *Acta Crystallogr., Sect. A,* 2008, **64**, 112.

Table S1: Metal-ligand bond distances (Å) in the structure of *fac*-$[Ru(L^{ph})_3][PF_6]_2$• acetone

Ru(1)–N(11B)	2.062(12)
Ru(1)–N(22C)	2.070(12)
Ru(1)–N(11A)	2.075(11)
Ru(1)–N(22A)	2.092(12)
Ru(1)–N(11C)	2.100(11)
Ru(1)–N(22B)	2.103(12)

Table S2: Metal-ligand bond distances (Å) in the structure of $[Ru_4Ag_6(L^{Ph})_{12}](PF_6)_{14}$

Ag(1)-N(52D)	2.288(7)	Ru(1)-N(21B)	2.053(5)
Ag(1)-N(41C)	2.328(7)	Ru(1)-N(22C)	2.058(7)
Ag(1)-N(52C)	2.332(6)	Ru(1)-N(11A)	2.073(7)
Ag(1)-N(41D)	2.354(7)	Ru(1)-N(11C)	2.087(5)
Ag(2)-N(52F)	2.288(7)	Ru(1)-N(11B)	2.095(6)
Ag(2)-N(52F)#1	2.288(12)	Ru(1)-N(22A)	2.096(7)
Ag(2)-N(41F)#1	2.328(7)	Ru(2)-N(22D)	2.051(7)
Ag(2)-N(41F)	2.328(7)	Ru(2)-N(22F)	2.049(6)
Ag(3)-N(41B)#1	2.317(6)	Ru(2)-N(22E)	2.052(7)
Ag(3)-N(41B)	2.317(6)	Ru(2)-N(11F)	2.080(7)
Ag(3)-N(52B)	2.330(7)	Ru(2)-N(11D)	2.094(5)
Ag(3)-N(52B)#1	2.330(12)	Ru(2)-N(11E)	2.120(7)
Ag(4)-N(41E)	2.293(6)		
Ag(4)-N(52A)	2.299(7)		
Ag(4)-N(41A)	2.308(6)		
Ag(4)-N(52E)	2.321(6)		

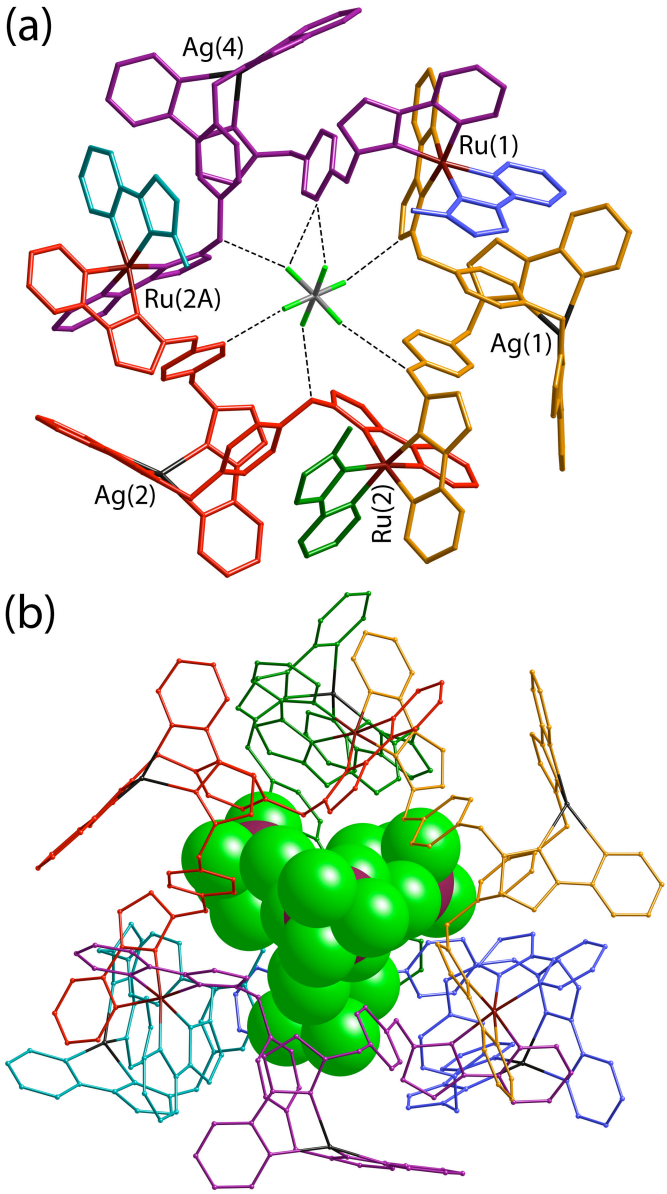

Figure S1. Two illustrations of how the encapsulated $[PF_6]^-$ anions interact with the cavity of the cage of $[\{Ru(L^{ph})_3\}_4Ag_6](PF_6)_{14}$. (a) Location of one of the anions in the window in the centre of a Ru_3Ag_3 face with some of the shorter CH•••F interactions (C•••F separation ≤ 3.15 Å) shown by dotted lines; (b) a view of the cage (in wireframe mode) with the four anions shown in space-filling mode.

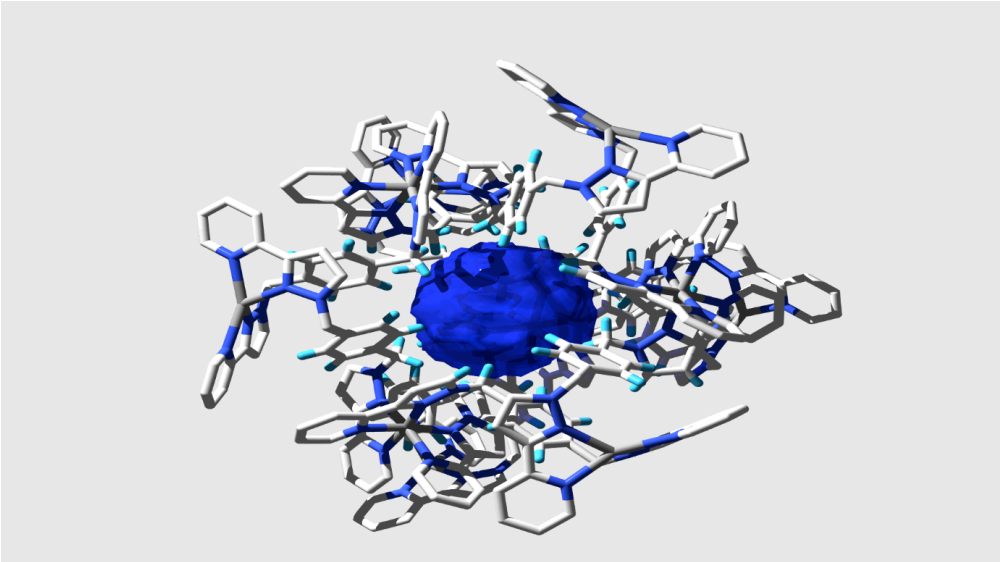

Figure S2. A view of the cavity in the centre of $[\{Ru(L^{ph})_3\}_4Ag_6](PF_6)_{14}$, shown in blue (generated with Swiss-PDB viewer, ref. S2).

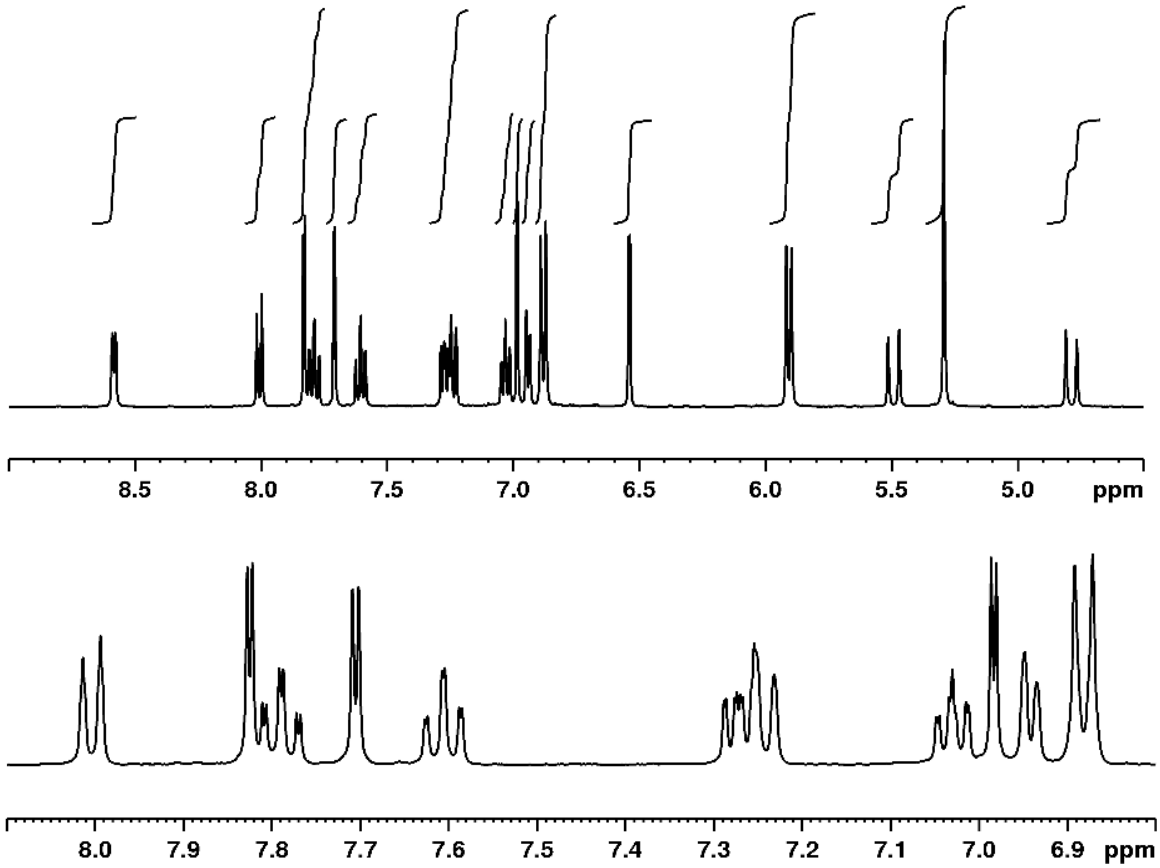

Figure S3. ^{1}H NMR spectrum of *fac*–$[Ru(L^{ph})_3][PF_6]_2$ (MeCN, 400 MHz, RT). Top: complete spectrum. Bottom: expansion of central region. Assignments (given with experimental details) were made on the basis of the COSY spectrum (Fig. S4).

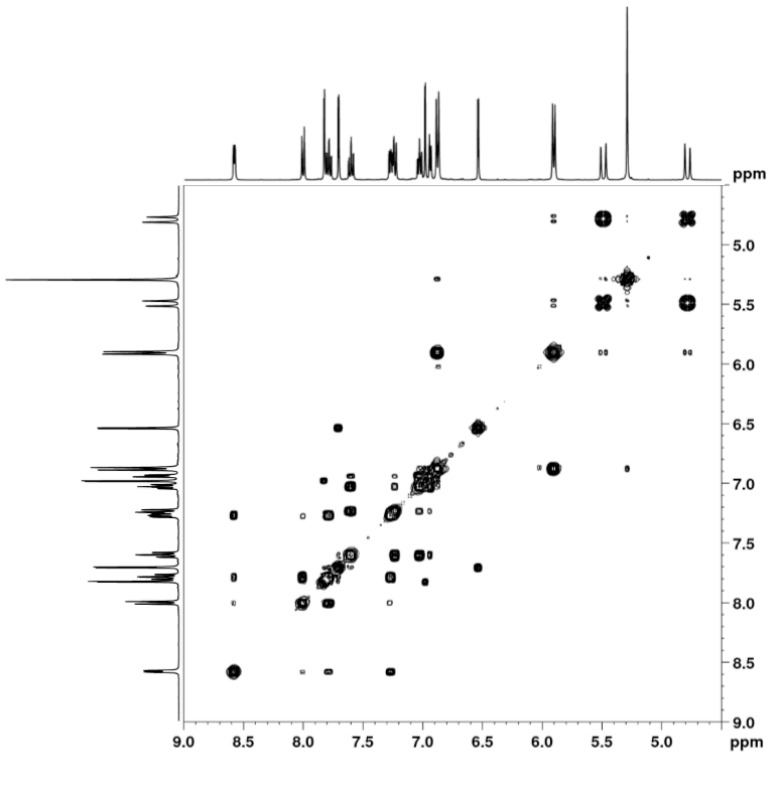

Figure S4. ^{1}H–^{1}H COSY spectrum of *fac*–$[Ru(L^{ph})_3][PF_6]_2$ (MeCN, 400 MHz, RT).

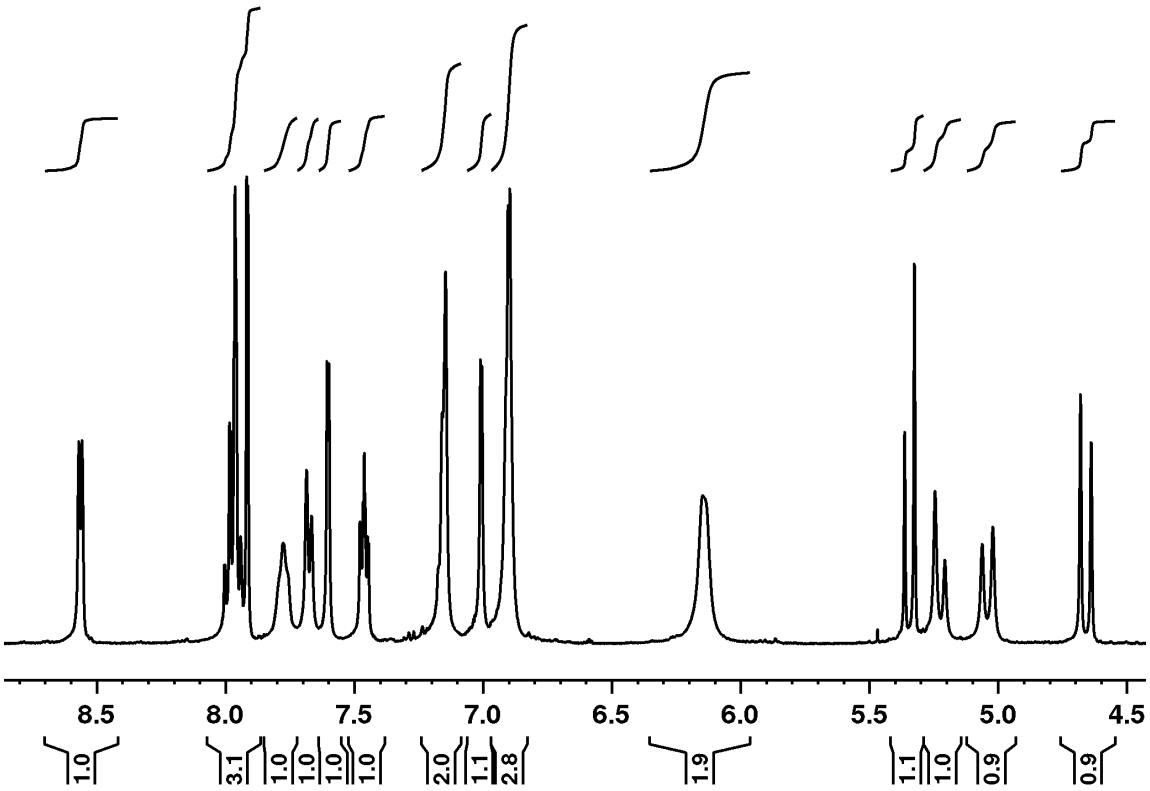

Figure S5. ^{1}H NMR spectrum of $[\{Ru(L^{ph})_3\}_4Ag_6](PF_6)_{14}$ (MeCN, 400 MHz, 75 °C).

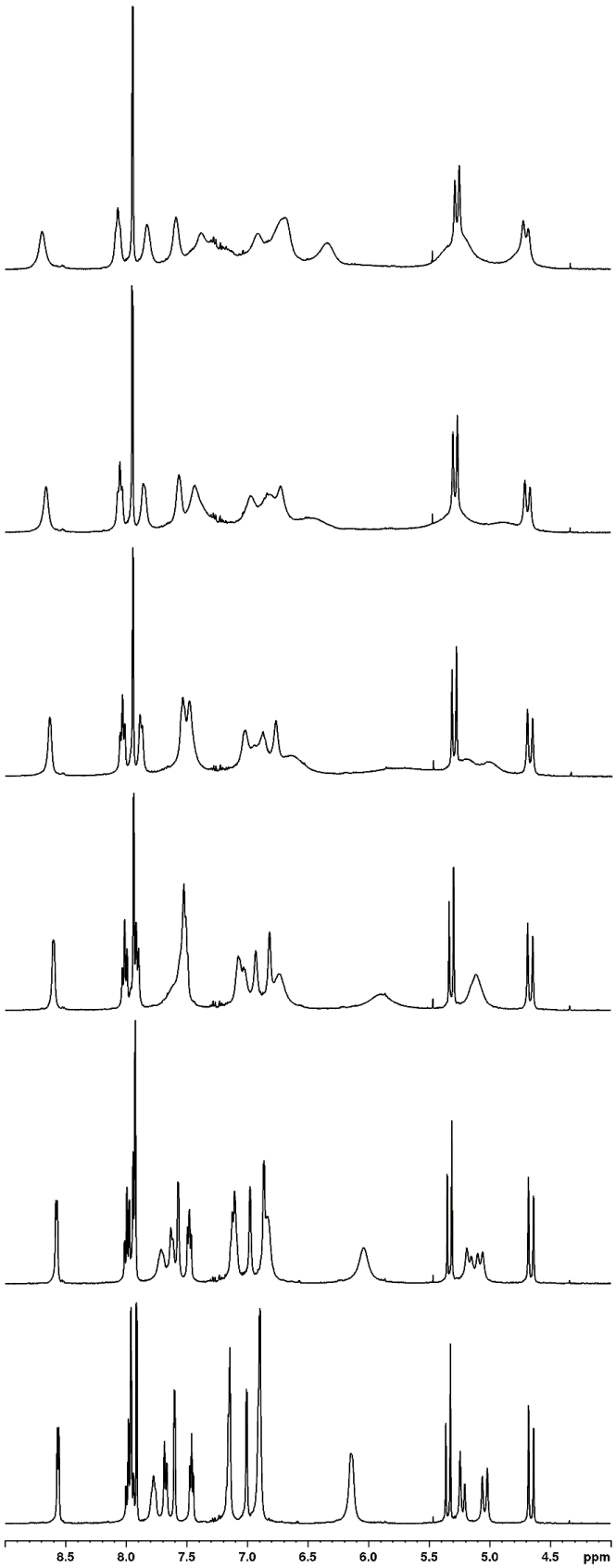

Figure S6. Series of ^{1}H NMR spectra of $[\{Ru(L^{ph})_3\}_4Ag_6](PF_6)_{14}$ (MeCN, 400 MHz) at (from top down) 25, 35, 45, 55, 65, 75˚C showing the sharpening at higher temperatures.

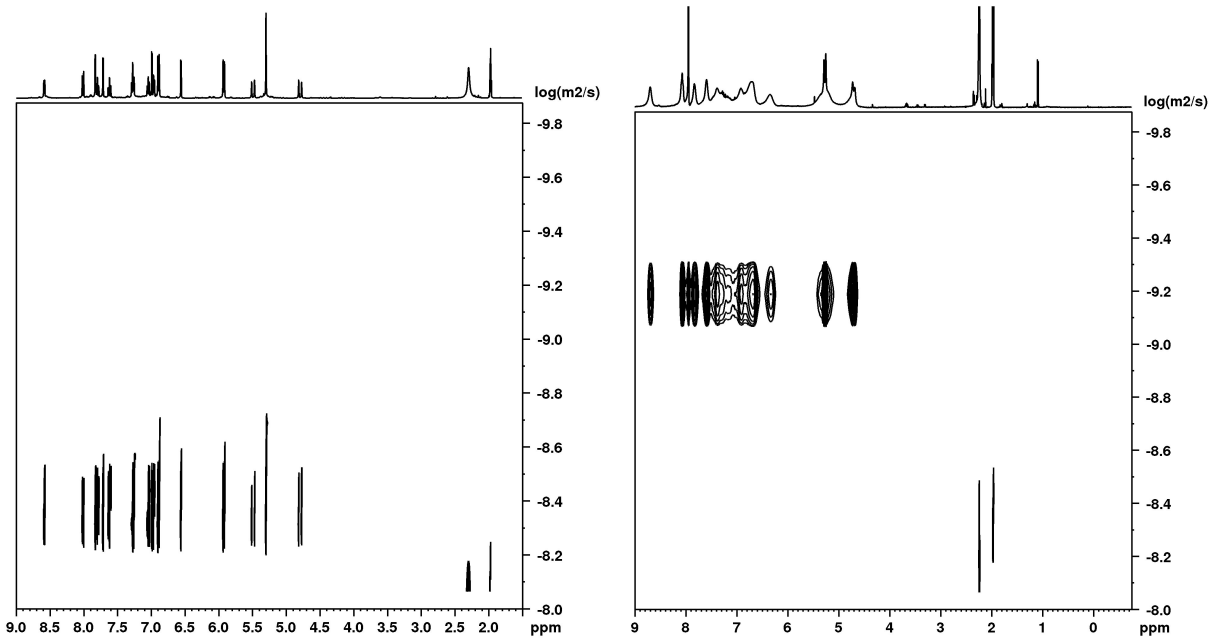

Figure S7. DOSY ^{1}H NMR spectra (MeCN, 400 MHz, RT) of *fac*–$[Ru(L^{ph})_3][PF_6]_2$ (left) and $[\{Ru(L^{ph})_3\}_4Ag_6](PF_6)_{14}$ (right)